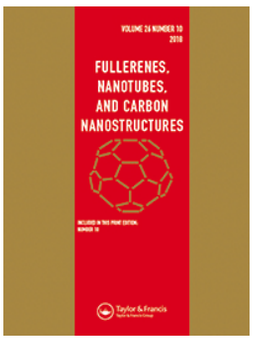

Fullerenes, Nanotubes and Carbon Nanostructures

ISSN: 1536-383X (Print) 1536-4046 (Online) Journal homepage: http://www.tandfonline.com/loi/lfnn20

Different dispersion states of MWCNT in aligned conductive electrospun PCL/MWCNT composites

Fabricio Molinari, Anahí V. Medrano, Alejandro Bacigalupe, Mariano M. Escobar & Leandro N. Monsalve

To cite this article: Fabricio Molinari, Anahí V. Medrano, Alejandro Bacigalupe, Mariano M. Escobar & Leandro N. Monsalve (2018) Different dispersion states of MWCNT in aligned conductive electrospun PCL/MWCNT composites, Fullerenes, Nanotubes and Carbon Nanostructures, 26:10, 667-674, DOI: 10.1080/1536383X.2018.1463994

To link to this article: https://doi.org/10.1080/1536383X.2018.1463994

FULLERENES, NANOTUBES AND CARBON NANOSTRUCTURES
2018, VOL. 26, NO. 10, 667–674
https://doi.org/10.1080/1536383X.2018.1463994

Taylor & Francis
Taylor & Francis Group

Different dispersion states of MWCNT in aligned conductive electrospun PCL/MWCNT composites

Fabricio Molinari[a], Anahí V. Medrano[b], Alejandro Bacigalupe[c], Mariano M. Escobar[c,d], and Leandro N. Monsalve [b,d]

[a]INTI Textiles – Av. Gral. Paz 5445 (B1650WAB), San Martín, Buenos Aires, Argentina; [b]INTI CMNB – Av. Gral. Paz 5445 (B1650WAB), San Martín, Buenos Aires, Argentina; [c]INTI Caucho – Av. Gral. Paz 5445 (B1650WAB), San Martín, Buenos Aires, Argentina; [d]CONICET – INTI – Av. Gral. Paz 5445 (B1650WAB), San Martín, Buenos Aires, Argentina

ABSTRACT

This work presents the synthesis and characterization of oriented nanofibers made of polycaprolactone (PCL) and multiwalled carbon nanotubes (MWCNT) obtained by electrospinning. The preparation of MWCNT/PCL solutions and electrospinning conditions were studied in order to maximize electrical conductivity of the composite and fiber alignment. The characterization of MWCNT/PCL solutions and fibers revealed the occurrence of different dispersion states for MWCNTs for different loads, which in turn affected the properties of the electrospun composite, such as its double electrical percolation and the in-fiber orientation of the PCL crystals. As the same dispersion states of MWCNT were present in both PCL/MWCNT dispersions and fibers, the rheology of the former can be correlated to the final properties of the latter.

ARTICLE HISTORY
Received 5 April 2018
Accepted 8 April 2018

KEYWORDS
Conductive nanofibers; electrospinning; rheology; carbon nanotubes; polycaprolactone

1. Introduction

During the last few decades, interest in electrically conductive fibers has increased markedly in areas such as medicine, sports, military, and energy. These fibers have been featured extensively as power and signal transmitters for ECG measurement,[1] strain sensors,[2] devices for electrotherapy,[3] pressure sensors,[4] chemical sensors,[5] and photovoltaic devices.[6] The electrospinning technique is a suitable method for the fabrication of fibers from melt or solution-processed materials by means of an electric field applied between a source (usually a needle) from which the material flows, and a collector.

Polycaprolactone (PCL) has been extensively used alone and in combination with other polymers for the fabrication of electrospun fibers.[7,8]Herrero et al.[9] evaluated the main electrospinning parameters using a poly(lactic acid) and polycaprolactone mixture: polymer concentration in the injectable solution, solvents used and their proportion, flow rate, voltage and distance to collector.[9]

Lee et al. studied PCL in combination with 3-polyhexylthiophene (P3HT) in order to improve the quality of the fibers compared to P3HT alone.[7] Zhou et al. developed highly hydrophilic hollow PCL microfibres by the co-electrospinning of PCL-polysiloxane-based surfactant (PSi) as building elements to create tissue-mimicking test objects (phantoms) for validation of diffusion magnetic resonance imaging (MRI).[10]

PCL concentration is a key parameter in the preparation of fibers by electrospinning. It has been reported that solutions between 10 wt.% and 15 wt.% of PCL were used to obtain fibrous structures.[11,12] Different solvents were tested for fiber preparation by electrospinning process, such as: DMF, chloroform, and solvent mixtures such as chloroform: methanol.[12–15]

Multiwalled carbon nanotubes (MWCNT) have been employed along with PCL for the preparation of polymer composites with enhanced mechanical properties, chemical stability and electrical conductivity. These composites have potential applications in electro-active devices,[16] controlled release and tissue engineering.[14] Moreover, they have been processed by electrospinning.[12,14]

Regarding the dispersion of MWCNTs, many approaches have been used: covalent modification of MWCNT surface[12,16,17] or use of different surfactants such as dodecyl sodium sulfonate, Pluronics, Triton X-100 and polyvinylpyrrolidone (PVP).[18–20] More recently, Fernández et al. evaluated the mechanical properties and fatigue analysis of poly(ε-caprolactone)-carbon nanotube composite scaffolds to be used in tissue engineering.[21] Liao et al. fabricated aligned poly(L-lactide) (PLLA)/poly(ε-caprolactone) (PCL)/functionalized multiwalled carbon nanotube (F-MWNT) composite fibrous membranes by electrospinning.[22]

The present work shows the relationship between the rheological behavior of the PCL with different amount of MWCNT and the final structure of electrospun fiber. The physical, morphological and electrical properties were characterized. The MWCNT dispersion, alignment and nucleating effects of MWCNT on PCL were observed. The electrical properties of the composite fibers were related to the dispersion degree of MWCNT and thus to their morphological, thermal and spectroscopic properties.

CONTACT Leandro N. Monsalve monsalve@inti.gob.ar Av. Gral. Paz 5445 ed. 42 piso 1 (B1650WAB) San Martín, Buenos Aires, Argentina.
Color versions of one or more of the figures in the article can be found online at www.tandfonline.com/lfnn.

2. Experimental

PCL (Mw 80000, Sigma-Aldrich), polyvinyl pyrrolidone PVP K30 (Anedra, Argentina), MWCNT (Nanocyl 7000), and DMF were reagent grade and used straight from the bottle.

2.1. Solutions preparation

Different amounts of MWCNTs (0-0.7 g) were dispersed in 100 ml of DMF and sonicated at 120 W for 15 minutes, followed by magnetic stirring for 15 minutes. After that, equal mass of PVP (a nonionic surfactant) to that of MWCNTs was added. The dispersion was sonicated again for about 20 minutes in an Omni-ruptor 4000 probe sonicator.

PCL/MWCNT solution were prepared dissolving 4.4 g of PCL into 20 g of the dispersion under magnetic agitation at 45°C for 4 h. Regarding PCL content, the solution concentration was 18 wt.%.

Dispersions with different MWCNT contents were electrospun: 0, 0.5, 0.9, 1.3, 1.8, 2.2 and 3.0 wt.% respect to total solids content (MWCNT+PCL+PVP).

2.1.1. Electrospinning conditions

A Y-flow electrospinner 2.2.D-500 was used for electrospinning. Distance between the needle and the collector was 26 cm. The flow rate of the solution was 1 ml h^{-1} for all samples. A rotary drum collector was employed in order to produce mats of aligned fibers. The setup included two high voltage sources: one at the needle between of +6 and +12 KV and the other at the collector between of −15 and −17 KV. Preliminary tests showed that fiber alignment increased with rotation speed. However, rotation speeds above 1000 RPM induced turbulent air stream that threw the fibers out of the collector.

2.1.2. Characterization

Viscosity was measured at 25 ± 0.1°C, over a shear rate range of 0.01-500 s^{-1} using a Physica MCR301 oscillatory rheometer (Anton Paar GmbH) equipped with concentric-cone geometry (CC27). Viscoelastic properties were evaluated through amplitude sweep test at 10 s^{-1} over a strain range of 0.01-500% on an oscillatory test equipped with cone-plate geometry (CP50) at 25 ± 0.1°C.

PCL/MWCNT solution was spun onto interdigitated gold electrodes of different width to length (W/L) ratio (L = 1-100 μm, W/L = 50-2000) patterned on a Si/SiO_2 (150 nm) substrate for 15 minutes using a rotary collector in order to align the fibers perpendicular to electrode fingers. A voltage sweep from 2 to −2 V was applied between electrodes. Resistance was calculated from the slope of current vs. voltage plot in the linear region near zero voltage.

Scanning electron microscopy was performed in a Zeiss Leo 982 Gemini (Carl Zeiss SMT GmbH). Focused Ion Beam (FIB) experiments were performed in a Helios Nanolab 650 (FEI). Fiber diameter measurement was carried out by analysis of SEM images using Image J software.[23] Statistics on results were performed using Minitab software aiming to determine the diameter distribution and differences between different content of MWCNT into the fibers. DSC was performed in a TA Q2000 from −90 to 100°C and from 100 to −90°C at 10°C/min. FTIR experiments were performed in a Shimadzu FTIR-8300 spectrophotometer in film with a ZnSe attenuated total reflectance (ATR) cell.

3. Results and discussion

3.1. Rheology of polymer solutions

Viscosity is a key parameter in the electrospinning technique. Figure 1 present viscosity as function of shear rate of PCL/MWCNT dispersions with different MWCNT contents. Dispersion with concentration greater than 3 wt.% MWCNT could not be electrospun due to their high viscosity. It is important to remark that this value is higher than that reported previously by Saeed et al., which used 2 wt.% for an electrospun PCL/MWCNT system as maximum content of MWCNT.[12]

The solution without MWCNT showed a Newtonian behavior for the whole shear rates range. The addition of 0.5 wt.% MWCNT caused an increase of the viscosity while keeping the Newtonian behavior of the solution. Samples with higher MWCNT content showed a shear thinning behavior.

The shear viscosity vs. shear rate can also be analyzed by the Ostwald I method (power-law) in the range of shear rate from 1 to 100 s^{-1}.

$$\ln(\tau) = \ln(a) + b \cdot \ln(\dot{\gamma}) \quad (1)$$

Where τ is the shear stress (Pa), $\dot{\gamma}$ is the shear rate (s^{-1}), a is the flow consistency index (Pa.s) and b is the flow behavior index. Table 1 shows values of a and b for all samples. Based on these parameters, suspensions containing 0 wt.% and 0.5 wt.% MWCNT presented ideal viscous flow behavior ($b = 1$), while for the samples with 1.8 wt.% and 3.0 wt.% MWCNT the value of b was lower than 1. Moreover, it can be seen that the pseudoplastic character of the suspension increased with concentration of MWCNT ($b_{0\%} > b_{0.5\%} > b_{1.8\%} > b_{3.0\%}$).

Figure 2a shows tan δ vs. strain for different PCL/MWCNT suspensions. At cross-over point (tan $\delta = 1$), the system passes from an elastic solid behavior (G′>G″) to a viscous liquid

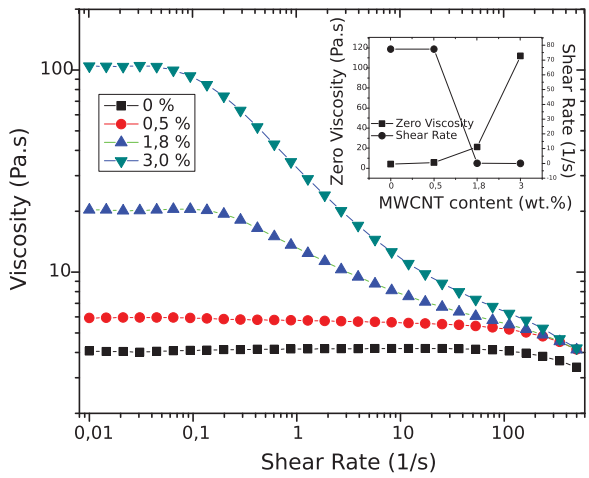

Figure 1. Shear Viscosity and Zero Shear Viscosity values of PCL/MWCNT suspensions. The MWCNT load is expressed as fraction of total solids content of each solution.

Table 1. Power law analysis for samples with different MWCNT contents.

Sample	*a*	*b*	R^2
0%	4.179	0.999	0.999
0.5%	5.184	0.982	0.999
1.8%	12.364	0.815	0.999
3.0%	28.434	0.646	0.987

Table 2. Rheological analysis data for PCL/MWCNT suspensions. The MWCNT load is expressed as fraction of total solids content of each solution.

Sample	LVE (%)	G'_{LVE} (Pa)	Flow Point (Pa)
0%	100.00	0.62	—
0.5%	32.54	140.50	64.77
1.8%	0.63	279.90	2.51
3.0%	0.22	421.20	1.34

(G″>G′). The value of shear stress where tan $\delta = 1$ is known as flow point, and represents the amount of energy needed to start flowing. Sample without MWCNT exhibited a viscous liquid behavior throughout the test (tan $\delta > 1$). The incorporation of MWCNT induced a solid elastic behavior at low deformation due to the ability of nanotubes to entwine and form a coupled network that keeps the applied deformation within the elastic range.[24] Figure 2b presents the storage modulus G′ as a function of shear stress.

Table 2 shows linear viscoelastic (LVE) range, storage modulus at LVE range (G'LVE) and flow point values. The LVE range represents the region where G′ and G′ remains constant under applied deformation. Typically, storage modulus is the most sensitive to the LVE range, and G'LVE symbolizes G′ values where LVE is exceeded. Finally, flow point indicates the critical level of stress that must be reached in order to start flowing. The LVE range moved to lower values with the addition of MWCNT.

Shear thinning behavior of PCL/MWCNT dispersions occur mostly due to the interaction between the MWCNT themselves. This interaction can be evidenced by the appearance of zero shear viscosity plateau at low shear rate due to the formation of entanglements in the suspension of MWCNT that is stabilized van der Waals type interactions.[25]

Around zero shear rate, the strain is not enough to alter the structural network. Moreover, at higher MWCNT content, the zero shear viscosity plateau decays at lower shear rate. This transition to shear thinning behavior happens at lower shear rates for more concentrated solutions, because they are more prone to greater entanglement. This phenomenon was reported in several works,[26–28] where it is mentioned that increasing the rod-like nanoparticles content produces stronger shear thinning behavior and higher zero shear viscosity. The applied shear rate causes disentanglements and disintegration of the agglomerates, and orientation of the MWCNT with the external force.

The increase of G′ with MWCNT content can be explained taking into account two different contributions: on one hand, the dispersion of MWCNT contributes to the elastic behavior of the sample and, on the other hand, the ability of MWCNT as nucleating agent to crystallize PCL.[29]

The occurrence of different dispersion states in both PCL/MWCNT dispersions and fibers could be verified by different methods. The decay of LVE with MWCNT content (Table 2) can be related to the dispersion degree of nanotubes: when agglomeration degree is higher, their efficiency as nucleating agent decays. On the other hand, the incorporation of MWCNT produces an increase of G'_{LVE} caused by the entanglements between the nanotubes. Note that Yu et al. claim that large values of G′ promotes the formation of fibers by electrospinning rather than drops.[30] Moreover, an increase in viscosity prevents the occurrence of beaded fibers structures that form due to the growth of capillary rupture instabilities while jets solidifies.[31]

3.2. Fiber characterization

Figure 3 shows SEM micrographs of aligned fibers with different MWCNT contents. Fibers without MWCNT presented a smooth surface, whereas those including MWCNTs showed a rough surface. This could be due to the interaction of DMF with the MWCNT surface and to the greater viscosity, hindering the evaporation of solvent during the fiber formation process. Additionally, SEM images reveal that fibers with 1.8 wt.% MWCNT are less aligned and more irregular than those with lower and higher MWCNT loads. Considering diameters of fibers with different MWCNT content, a sharp increase from 0.5 μm to 1.2 μm at 2.2 wt.% was observed (Table 3). SEM images with higher magnification allowed to distinguish MWCNT dispersed within the PCL.

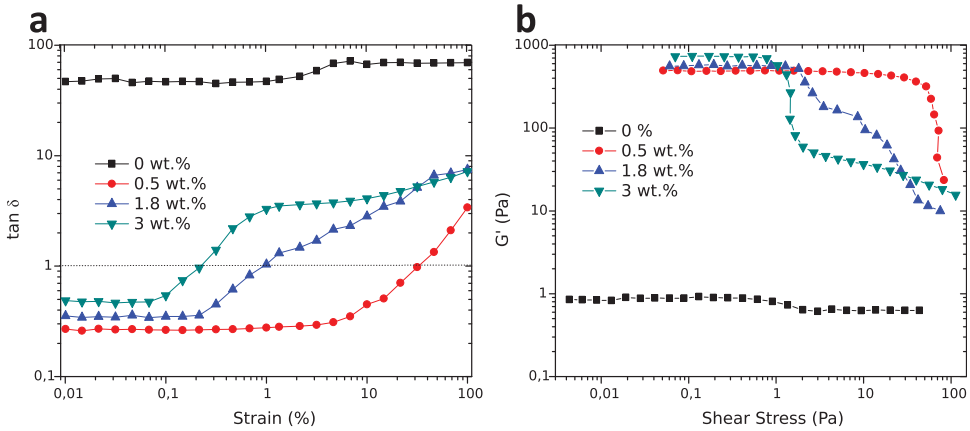

Figure 2. (a) Tan δ values as function of strain of PCL/MWCNT suspensions and (b) Storage modulus G′ as function of shear stress. The MWCNT content is expressed as fraction of total solids content of each solution.

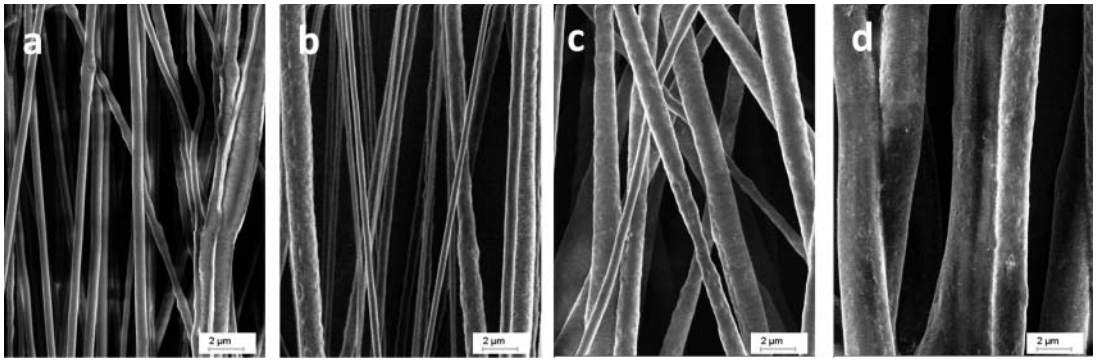

Figure 3. SEM images of electrospun fibers of PCL/MWCNT with different content of MWCNT: (a) 0 wt.%, (b) 0.5 wt.%, (c) 1.8 wt.% and (d) 3 wt.%.

Figure 4a exhibits partially aligned MWCNT parallel to the fiber axis, due to the flow of polymer solution through the needle and the electric field-mediated elongation during the fiber formation process. Cross sections of fibers with 3 wt.% MWCNT (Figures 4b and c) reveal the occurrence of two dispersion states of MWCNT: well dispersed and evenly distributed MWCNTs and aggregates.

SEM micrographs also support the presence of two dispersion states. This is in agreement with the results from strain-controlled tests of polymer solutions, which indicate that the presence of different dispersion states of MWCNTs in fibers are mainly due to the presence of the same dispersion states in polymer solutions rather than to an aggregation process during fiber formation. On the other hand, the presence of voids around MWCNT aggregates can be explained by the evaporation of DMF trapped in the MWCNT aggregates during fiber formation. A cross section of a PCL fiber without MWCNTs is also shown for comparison purposes (Figure 4d).

Melting temperature (T_m) and heat of fusion (ΔH_m) were determined from the DSC first heating runs of the samples. Crystallization temperature (T_c) and heat of crystallization (ΔH_c) were determined from the DSC cooling runs. Crystallinity was obtained using heat of fusion of pure PCL 139.5 J/g.[32] All Results are summarized in Table 4.

T_c increased with MWCNT loading. For instance, the sample with 3 wt.% MWCNT presented a T_c value 13°C higher than that without MWCNT. On the other hand, crystallinity values did not change significantly among the different samples. Melting point was not affected by the addition of MWCNTs until 1.8 wt.%. For higher content (2.2 wt.% and 3 wt.%), the melting point decreased slightly.

Regarding changes in melting point of the fibers, Kim et al.[33] showed that PVP can decrease the melting point of PCL due to its partial miscibility. However, in the present case, addition of PVP seems to affect slightly the melting point of the PCL composite fibers. This can be explained by intermolecular interactions in the ternary system PCL/MWCNT/PVP together with the dispersion state of MWCNT. A strong preference of PVP for MWCNTs prevents the former to interact with PCL and keeps the dispersion thermodynamically stable. As MWCNT concentration increases, some aggregates can be formed (for concentration higher than 1.3 wt.% according to nucleation efficiency). Beyond 2.2 wt.%, MWCNT surface can be assumed to be saturated with PVP (the same amount of PVP and MWCNT was added in each case) and the remaining PVP interacts with PCL, decreasing its melting point.

Table 3. Average diameter of electrospun fiber with different MWCNT contents.

MWCNT content [%wt]	0	0.5	0.9	2.2	3.0
Average diameter [nm]	460 ± 16	569 ± 18	505 ± 16	1120 ± 30	1370 ± 30

Nucleation efficiency (*NE*) is one of the best ways to quantitatively assess the nucleation capacity of an additive to act as nuclei for the crystallization of a given polymer compared to self-nucleation. The self-nucleation scale for PCL/MWCNT composites was employed as used by Pérez et al.[34] The nucleation efficiency can be calculated according to the following expression:

$$NE = \frac{T_{c,NA} - T_{c,PCL}}{T_{c,max} - T_{c,PCL}} \times 100 \quad (2)$$

where $T_{c,NA}$ is the peak T_c value determined in a DSC cooling run for a sample of the polymer with the nucleating agent (NA), $T_{c,PCL}$ is the peak T_c value for neat PCL, and $T_{c,max}$ is the maximum peak crystallization temperature determined after neat PCL has been self-nucleated at the ideal self-nucleation temperature or $T_{s,ideal}$ (i.e., the self-nucleation temperature that produces maximum self-nucleation). The values of $T_{s,ideal}$ and $T_{c,max}$ were determined according to Trujillo et al.[35] (See supplementary information for experimental details).

Figure 5 presents *NE* values, which increase with MWCNT content. Moreover, *NE* values higher than 100% demonstrate supernucleation effects.

Supernucleation effects have been already reported for PCL/MWCNT composites[35] and indicate that the MWCNT surface is a better nucleation agent for PCL than the PCL crystal itself. The increasing trend of *NE* with the addition of MWCNTs can be explained by the surface area of rod-like nanoparticles, which promotes the crystallization mechanism.*NE* rapidly grows up to 231% for a MWCNT content of 1.3 wt.%. Beyond this content, NE remains almost constant. This fact can be attributed to the presence of different dispersion states, as deduced from rheological and microscopy measurements. For loads above 1.3 wt.%, MWCNT aggregates begin to form and thus part of their surface is no longer available for the crystallization of PCL. Therefore, this eventually leads to a decoupling between MWCNT load and *NE*.

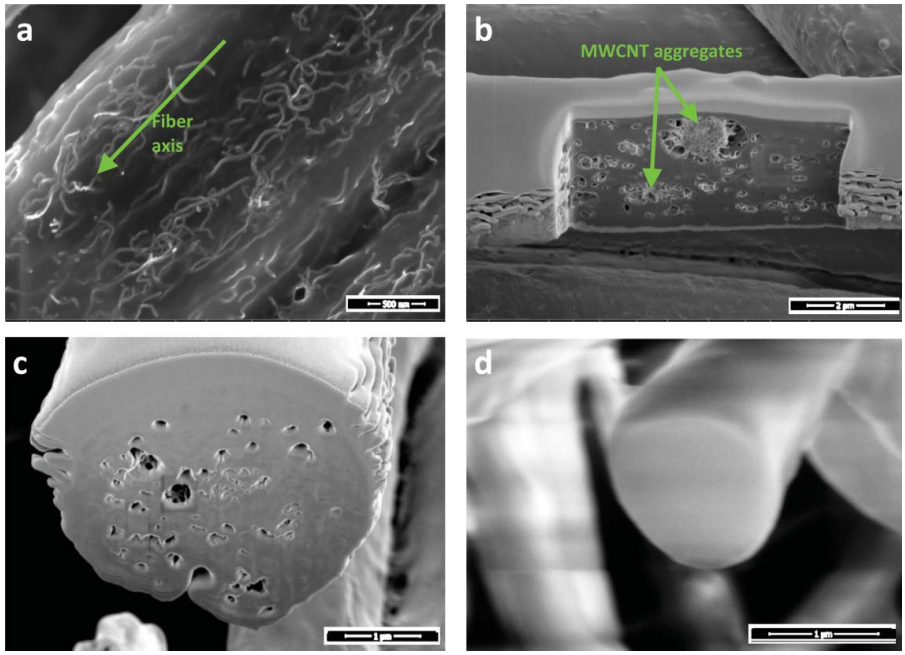

Figure 4. SEM image of (a) PCL fiber with 3% MWCNT; (b,c) Cross sections of PCL/MWCNT fiber; (d) A cross section of a PCL fiber without MWCNT.

Electrospun fibers were also characterized by FTIR (Figure 6). FTIR spectra show characteristic signals of PCL. Among them, a strong absorption peak at 1718 cm^{-1} (C=O stretch) and two bands between 1120 and 1200 cm^{-1} (C-(C=O)-O axial deformation) showed changes with the addition of MWCNTs. C=O stretch band shifted to 1723 cm^{-1} as MWCNT concentration increased up to 1.3 wt.%. Further increase in concentration induced a shift of this band to 1720 cm^{-1}. Similar behavior was found for band at 1155 cm^{-1}, which shifted to 1165 cm^{-1} when MWCNT concentration increased from 0 to 1.3 wt.%. After that, this band shifted back to lower wavenumbers with further MWCNT addition. Moreover, a relative decrease in intensity of the latter band compared to the partially overlapped shoulder at 1190 cm^{-1} has been noticed. Changes in FTIR band shift and intensity of PCL have been associated to crystalinity[36] but also to crystal orientation.[37] In our case, the manufacture process produced aligned fibers with MWCNT partially aligned along the fiber axis, as seen in SEM images. DSC experiments demonstrated that MWCNTs act as nucleating agents. Therefore, changes in the above-mentioned FTIR bands can be assumed to occur due to changes in preferred orientation for crystallization of PCL. MWCNT addition up to 1.3 wt.% leads to a well dispersed and aligned crystallization nuclei in the fiber and thus there is a preferred orientation for the PCL crystals. When MWCNT concentration increases, further aggregates start to occur and, due to their lower length-to-diameter ratio compared to isolated MWCNT growth direction of the PCL, crystals is no longer determined by isolated and aligned MWCNTs.

Table 4. Melting temperature, crystallization temperature, heat of fusion and crystallization, crystallinity for electrospun PCL fibers with different MWCNT content.

MWCNT content (%)	T_m (°C)	ΔH_m (J/g)	T_c (°C)	ΔH_c (J/g)	Crystallinity (%)
0	59.26	69.4	29.60	55.2	49.7
0.5	59.10	68.1	33.70	53.7	48.8
0.9	59.19	70.3	35.26	55.5	51.8
1.3	59.34	71.8	41.60	55.9	51.5
1.8	59.58	69.3	42.28	55.4	49.7
2.2	58.48	70.3	39.26	53.9	50.4
3.0	57.46	74.3	42.60	61.2	53.3

Figure 7 presents sheet resistance (R_s) of aligned fiber mats in the direction of fiber orientation as a function of MWCNT content. Two percolation zones could be observed. R_s decreases about 1 order of magnitude with the addition of 0.9 wt.% MWCNT and up to three orders with 1.8 wt.% MWCNT. An abrupt decrease in 6 orders of magnitude with 2.2 wt.% MWCNT load was observed. This fact is in agreement with the occurrence of two dispersion states in the composite: one, of well dispersed MWCNTs which are indirectly contacted by tunneling through the polymer matrix, and the other, made of aggregates in direct contact which form discrete conductive paths through the polymer matrix.

If the MWCNT content is assumed to be homogeneous, the composite conductivity (σ) can be explained by a single tunnel

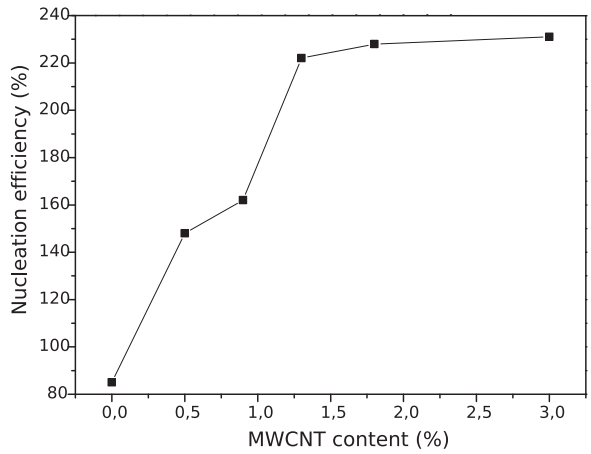

Figure 5. Nucleation efficiency vs. MWCNT content for electrospun PCL/MWCNT composites.

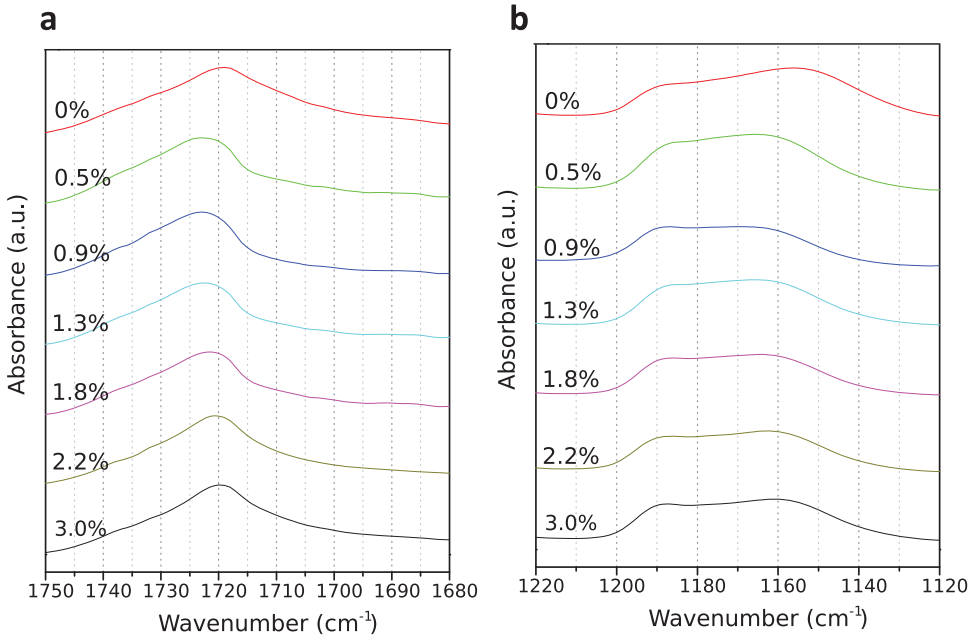

Figure 6. FTIR carbonyl stretching (a) and carbonyl axial deformation (b) of PCL from aligned electrospun fibers with different MWCNT content.

junction where the gap width (w) varies linearly with MWCNT$^{-1/3}$. It can also be demonstrated that $\ln(\sigma) \propto -w$ and thus $\ln(\sigma) \propto -\text{MWCNT}^{-1/3}$.[38,39] Moreover, considering that $R_s \propto \sigma^{-1}$ given that deposition time and flow rate of solution were kept constant, it can be concluded that:

$$\ln(R_s) \propto MWCNT^{-1/3} \quad (3)$$

A linear behavior for the logarithm of R_s vs MWCNT $^{-1/3}$ could be observed in the inset of Figure 7 for 0.9, 1.3 and 1.8 wt.% MWCNT loads.

Sheet resistivity for a sample containing 3 wt.% MWCNT was 4.2 ± 0.7 MΩ/sq. Volume resistivity is difficult to estimate since the surface of the electrodes has not been fully covered. However, using electrodes of high W/L ratio, a resistance of few kΩ could be measured, which is adequate for the application of a thin layer of these conductive fibers for the fabrication of flexible electronic devices.

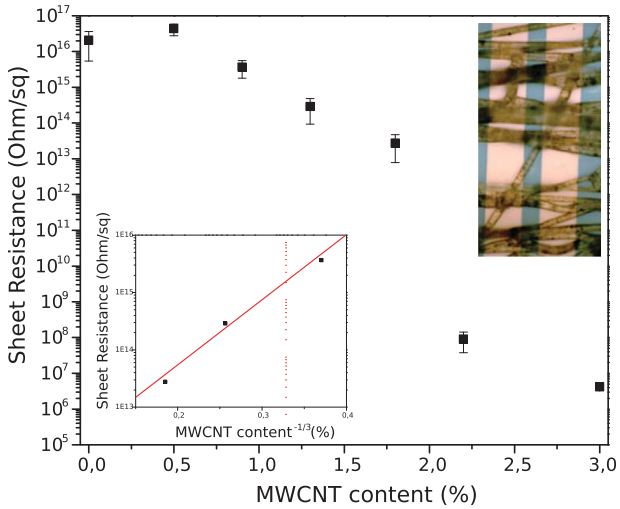

Figure 7. Sheet resistivity of electrospun PCL/MWCNT aligned fiber composites along the orientation axis as a function of carbon nanotube loading. In the left lower inset, the points between first and second percolation were plotted as a function of MWCNT content $^{-1/3}$. The inset on the right is an optical image of the fibers deposited onto electrodes (L = 10 μm). Deposition time was 15 minutes.

Two percolation thresholds for polymer composites filled with conductive particles were already observed and modeled in previous studies.[40,41] This behavior has been explained by both geometrical factors and processing conditions. In our case, fibers are composed of non-spherical conductive fillers with different possible contact configurations (edge to edge, edge to sidewall and sidewall to sidewall). Moreover, MWCNTs are aligned along the fiber axis due to the electrospinning procedure. The first percolation threshold (between 0.5 wt.% and 0.9 wt.%) can be assumed to be due to edge to edge contacts, and the second percolation threshold (around 1.8 wt.% by weight) to be due to sidewall to sidewall contacts. When these types of contacts begin to occur, aggregation of MWCNTs also becomes noticeable. Also, the occurrence of carbon nanotube aggregates in a polymer matrix led to a major change in resistivity of the fiber composite. This fact has been previously observed and discussed by other authors.[42] The explanation for that phenomenon is that once the percolation threshold was reached, the contact area between aggregated MWCNTs is larger than for well-dispersed MWCNTs. Moreover, a large change in both fiber resistivity and diameter took place at the same concentration. Therefore, changes in fiber diameter can be concluded to be mainly associated to changes in fiber conductivity. Conductive fibers accumulate less electrostatic charge and thus experiment less stretching force during fiber elongation process. Also around the second percolation threshold (1.8 wt.%) the instability of the conductivity generates sudden changes in the stretching forces, yielding more irregular fibers.

4. Conclusion

Conductive electrospun PCL/MWCNT composites could be fabricated using a flexible and biodegradable polymer and a

metal-free conductive addition. Electrospinning conditions were studied in order to obtain regular fibers with well dispersed MWCNTs without any chemical treatment.

Partial alignment and the occurrence of two dispersion states for MWCNT had an important effect on composite properties such as resistivity and polymer crystal orientation. All characterization methods employed in this work (Rheology, SEM/FIB images, DSC, FTIR and electrical properties) provided useful results in order to address dispersion state and partial alignment of MWCNT. Rheological characterization of PCL/MWCNT dispersions prior to fiber fabrication was especially important for addressing the right dispersion states for MWCNTs and achieving the desired final properties in conductive fibers. As a result, a simple and reproducible method has been used for the preparation of conductive electrospun PCL/MWCNT composites with potential application in flexible scaffolds for sensor and tissue engineering applications.

Acknowledgments

We thank INTI, ANPCyT (PICT 2013-0427 and PICT 2014–3748) for financial support. We thank Dr. Federico Golmar for the interdigitated electrodes, Sandra Jung for the statistics on fiber diameter and Mauro Fernández for FTIR spectra. LNM and MME are research staff of CONICET.

Funding

Fondo para la Investigación Científica y Tecnológica, PICT 2014-3748. Fondo para la Investigación Científica y Tecnológica, PICT 2013-0427.

ORCID

Leandro N. Monsalve http://orcid.org/0000-0001-9306-8618

References

[1] Truong, T. K.; Lee, Y.; Suh, D. Multifunctional characterization of carbon nanotube sheets, yarns, and their composites. *Curr. Appl. Phys.* **2016**, *16*, 1250–1258. DOI: 10.1016/j.cap.2016.04.023.

[2] Chilles, J. S.; Koutsomitopoulou, A. F.; Croxford, A. J.; Bond, I. P. Monitoring cure and detecting damage in composites with inductively coupled embedded sensors. *Compos. Sci. Technol.* **2016**, *134*, 81–88. DOI: 10.1016/j.compscitech.2016.07.028.

[3] Oh, K. W.; Park, H. J.; Kim, S. H. Stretchable Conductive Fabric for Electrotherapy. *J. Appl. Polym. Sci.* **2003**, *88*, 1225–1229. DOI: 10.1002/app.11783.

[4] Quandt, B. M.; Hufenus, R.; Weisse, B.; Braun, F.; Wolf, M.; Scheel-sailer, A.; Bona, G.; Rossi, R. M.; Boesel, L. F. Optimization of novel melt-extruded polymer optical fibers designed for pressure sensor applications. *Eur. Polym. J.* **2017**, *88*, 44–55. DOI: 10.1016/j.eurpolymj.2016.12.032.

[5] Laxmeshwar, L. S.; Jadhav, M. S.; Akki, J. F.; Raikar, P.; Kumar, J. Highly sensitive fiber grating chemical sensors: An effective alternative to atomic absorption spectroscopy. *Opt. Laser Technol.* **2017**, *91*, 27–31. DOI: 10.1016/j.optlastec.2016.11.025.

[6] Bedeloglu, A.; Demir, A.; Bazkurt, Y.; Sariciftci, N. S. A Photovoltaic Fiber Design for Smart Textiles Smart Textiles and Photovoltaic Preparation of Photovoltaic Fiber Structure. *Text. Res. J.* **2010**, *80*, 1065–1074. DOI: 10.1177/0040517509352520.

[7] Lee, S.; Moon, G. D.; Jeong, U. Continuous production of uniform poly(3-hexylthiophene) (P3HT) nanofibers by electrospinning and their electrical properties. *J. Mater. Chem.* **2009**, *19*, 743. DOI: 10.1039/b814833c.

[8] Chen, M.-C.; Sun, Y.-C.; Chen, Y.-H. Electrically conductive nanofibers with highly oriented structures and their potential application in skeletal muscle tissue engineering. *Acta Biomater.* **2013**, *9*, 5562–5572. DOI: 10.1016/j.actbio.2012.10.024.

[9] Herrero Herrero, M.; Gómez-Tejedor, J. A.; Vallés-Lluch, A. PLA/PCL electrospun membranes of tailored fibres diameter as drug delivery systems. *Eur. Polym. J.* **2018**, *99*, DOI: 10.1016/j.eurpolymj.2017.12.045.

[10] Zhou, F.; Li, Z.; Gough, J. E.; Hubbard, P. L.; Parker, G. J. M. Axon mimicking hydrophilic hollow polycaprolactone micro fi bres for diffusion magnetic resonance imaging. *Mater. Des.* **2018**, *137*, 394–403. DOI: 10.1016/j.matdes.2017.10.047.

[11] Shao, S.; Li, L.; Yang, G.; Li, J.; Luo, C.; Gong, T.; Zhou, S. Controlled green tea polyphenols release from electrospun PCL/MWCNTs composite nanofibers. *Int. J. Pharm.* **2011**, *421*, 310–20. DOI: 10.1016/j.ijpharm.2011.09.033.

[12] Saeed, K.; Park, S.-Y.; Lee, H.-J.; Baek, J.; Huh, W. Preparation of electrospun nanofibers of carbon nanotube/polycaprolactone nanocomposite. *Polymer (Guildf).* **2006**, *47*, 8019–8025. DOI: 10.1016/j.polymer.2006.09.012.

[13] Doustgani, A.; Vasheghani-Farahani, E.; Soleimani, M.; Hashemi-Najafabadi, S. Optimizing the mechanical properties of electrospun polycaprolactone and nanohydroxyapatite composite nanofibers. *Compos. Part B Eng.* **2012**, *43*, 1830–1836. DOI: 10.1016/j.compositesb.2012.01.051.

[14] Shao, S.; Zhou, S.; Li, L.; Li, J.; Luo, C.; Wang, J.; Li, X.; Weng, J. Osteoblast function on electrically conductive electrospun PLA/MWCNTs nanofibers. *Biomaterials.* **2011**, *32*, 2821–2833. DOI: 10.1016/j.biomaterials.2011.01.051.

[15] Lee, S. W.; Lee, H. J.; Choi, J. H.; Koh, W. G.; Myoung, J. M.; Hur, J. H.; Park, J. J.; Cho, J. H.; Jeong, U. Periodic array of polyelectrolyte-gated organic transistors from electrospun poly(3-hexylthiophene) nanofibers. *Nano Lett.* **2010**, *10*, 347–51. DOI: 10.1021/nl903722z.

[16] Xiao, Y.; Zhou, S.; Wang, L.; Gong, T. Electro-active Shape Memory Properties of Poly(ε-caprolactone)/Functionalized Multiwalled Carbon Nanotube Nanocomposite. *ACS Appl. Mater. Interfaces.* **2010**, *2*, 3506–3514. DOI: 10.1021/am100692n.

[17] Vicentini, N.; Gatti, T.; Salice, P.; Scapin, G.; Marega, C.; Filippini, F.; Menna, E. Covalent functionalization enables good dispersion and anisotropic orientation of multi-walled carbon nanotubes in a poly(l-lactic acid) electrospun nanofibrous matrix boosting neuronal differentiation. *Carbon N. Y.* **2015**, *95*, 725–730. DOI: 10.1016/j.carbon.2015.08.094.

[18] Hasan, T.; Scardaci, V.; Tan, P.; Rozhin, A. G.; Milne, W. I.; Ferrari, A. C. Stabilization and "Debundling" of Single-Wall Carbon Nanotube Dispersions in N -Methyl-2-pyrrolidone (NMP) by Polyvinylpyrrolidone (PVP). *J. Phys. Chem. C.* **2007**, *111*, 12594–12602. DOI: 10.1021/jp0723012.

[19] Rastogi, R.; Kaushal, R.; Tripathi, S. K.; Sharma, A. L.; Kaur, I.; Bharadwaj, L. M. Comparative study of carbon nanotube dispersion using surfactants. *J. Colloid Interface Sci.* **2008**, *328*, 421–8. DOI: 10.1016/j.jcis.2008.09.015.

[20] Vaisman, L.; Wagner, H. D.; Marom, G. The role of surfactants in dispersion of carbon nanotubes. *Adv. Colloid Interface Sci.* **2006**, *128-130*, 37–46. DOI: 10.1016/j.cis.2006.11.007.

[21] Fernández, J.; Auzmendi, O.; Amestoy, H.; Diez-torre, A.; Sarasua, J. Mechanical properties and fatigue analysis on poly (ε – caprolactone) -polydopamine-coated nano fi bers and poly (ε – caprolactone) -carbon nanotube composite sca ff olds. *Eur. Polym. J.* **2017**, *94*, 208–221. DOI: 10.1016/j.eurpolymj.2017.07.013.

[22] Liao, G.; Zhou, X.; Chen, L.; Zeng, X.; Xie, X.; Mai, Y. Electrospun aligned PLLA / PCL / functionalised multiwalled carbon nanotube composite fibrous membranes and their bio / mechanical properties. *Compos. Sci. Technol.* **2012**, *72*, 248–255. DOI: 10.1016/j.compscitech.2011.11.009.

[23] Schneider, C. A.; Rasband, W. S.; Eliceiri, K. W. NIH Image to ImageJ: 25 years of image analysis. *Nat. Methods.* **2012**, *9*, 671–675. DOI: 10.1038/nmeth.2089.

[24] White, K. L.; Yao, H.; Zhang, X.; Sue, H. J. Rheology of electrostatically tethered nanoplatelets and multi-walled carbon nanotubes in

epoxy. *Polym. (United Kingdom).* **2016**, *84*, 223–233. DOI: 10.1016/j.polymer.2015.12.043.

[25] Girifalco, L. A.; Hodak, M.; Lee, R. S. Carbon nanotubes, buckyballs, ropes, and a universal graphitic potential. *Phys. Rev. B – Condens. Matter Mater. Phys.* **2000**, *62*, 13104–13110. DOI: 10.1103/PhysRevB.62.13104.

[26] Abraham, J.; Sharika, T.; Mishra, R. K.; Thomas, S. Rheological characteristics of nanomaterials and nanocomposites. In *Micro Nano Fibrillar Compos. (MFCs NFCs) from Polym. Blends*, Duxford: Elsevier, **2017**; pp 327–350. DOI: 10.1016/B978-0-08-101991-7.00014-5.

[27] Nobile, M. R. Rheology of polymer–carbon nanotube composites melts. In *Polym. Nanotub. Compos.*, Cambridge: Elsevier, **2011**; pp 428–481. DOI: 10.1533/9780857091390.2.428.

[28] Pötschke, P.; Fornes, T. D.; Paul, D. R. Rheological behavior of multiwalled carbon nanotube/polycarbonate composites. *Polymer (Guildf).* **2002**, *43*, 3247–3255. DOI: 10.1016/S0032-3861(02)00151-9.

[29] Zhou, B.; Tong, Z.-Z.; Huang, J.; Xu, J.-T.; Fan, Z.-Q. Isothermal crystallization kinetics of multi-walled carbon nanotubes-graft-poly (ε-caprolactone) with high grafting degrees. *CrystEngComm*. **2013**, *15*, 7824. DOI: 10.1039/c3ce40606g.

[30] Yu, J. H.; Fridrikh, S. V.; Rutledge, G. C. The role of elasticity in the formation of electrospun fibers. *Polymer (Guildf).* **2006**, *47*, 4789–4797. DOI: 10.1016/j.polymer.2006.04.050.

[31] Frenot, A.; Chronakis, I. Polymer nanofibers assembled by electrospinning. *Curr. Opin. Colloid Interface Sci.* **2003**, *8*, 64–75. DOI: 10.1016/S1359-0294(03)00004-9.

[32] Alp, B.; Cesur, S. Isothermal crystallization kinetics and mechanical properties of polycaprolactone composites with zinc oxide, oleic acid, and glycerol monooleate. *J. Appl. Polym. Sci.* **2013**, *130*, 1259–1275. DOI: 10.1002/app.39217.

[33] Kim, G. M.; Le, K. H. T.; Giannitelli, S. M.; Lee, Y. J.; Rainer, A.; Trombetta, M. Electrospinning of PCL/PVP blends for tissue engineering scaffolds. *J. Mater. Sci. Mater. Med.* **2013**, *24*, 1425–1442. DOI: 10.1007/s10856-013-4893-6.

[34] Pérez, R. A.; López, J. V.; Hoskins, J. N.; Zhang, B.; Grayson, S. M.; Casas, M. T.; Puiggalí, J.; Müller, A. J. Nucleation and Antinucleation Effects of Functionalized Carbon Nanotubes on Cyclic and Linear Poly(ε-caprolactones). *Macromolecules*. **2014**, *47*, 3553–3566. DOI: 10.1021/ma5005869.

[35] Trujillo, M.; Arnal, M. L.; Müller, A. J.; Mujica, M. A.; Urbina De Navarro, C.; Ruelle, B.; Dubois, P. Supernucleation and crystallization regime change provoked by MWNT addition to poly(ε-caprolactone). *Polymer (Guildf).* **2012**, *53*, 832–841. DOI: 10.1016/j.polymer.2011.12.028.

[36] Lee, K. S.; Chang, Y.-W. Thermal and mechanical properties of poly ((ε-caprolactone)/polyhedral oligomeric silsesquioxane nanocomposites. *Polym. Int.* **2013**, *62*, 64–70. DOI: 10.1002/pi.4309.

[37] Keroack, D.; Zhao, Y.; Prud'homme, R. E. Molecular orientation in crystalline miscible blends. *Polymer (Guildf).* **1998**, *40*, 243–251. DOI: 10.1016/S0032-3861(98)00187-6.

[38] Laredo, E.; Grimau, M.; Bello, A.; Wu, D. F.; Zhang, Y. S.; Lin, D. P. AC Conductivity of Selectively Located Carbon Nanotubes in Poly (ε-caprolactone)/Polylactide Blend Nanocomposites. *Biomacromolecules*. **2010**, *11*, 1339–1347. DOI: 10.1021/bm100135n.

[39] Kilbride, B. E.; Coleman, J. N.; Fraysse, J.; Fournet, P.; Cadek, M.; Drury, A.; Hutzler, S.; Roth, S.; Blau, W. J. Experimental observation of scaling laws for alternating current and direct current conductivity in polymer-carbon nanotube composite thin films. *J. Appl. Phys.* **2002**, *92*, 4024. DOI: 10.1063/1.1506397.

[40] Kovacs, J. Z.; Velagala, B. S.; Schulte, K.; Bauhofer, W. Two percolation thresholds in carbon nanotube epoxy composites. *Compos. Sci. Technol.* **2007**, *67*, 922–928. DOI: 10.1016/j.compscitech.2006.02.037.

[41] Nettelblad, B.; Mårtensson, E.; Önneby, C.; Gäfvert, U.; Gustafsson, A. Two percolation thresholds due to geometrical effects: experimental and simulated results. *J. Phys. D. Appl. Phys.* **2003**, *36*, 399. DOI: 10.1088/0022-3727/36/4/312.

[42] Aguilar, J. O.; Bautista-Quijano, J. R.; Avilés, F. Influence of carbon nanotube clustering on the electrical conductivity of polymer composite films. *Express Polym. Lett.* **2010**, *4*, 292–299. DOI: 10.3144/expresspolymlett.2010.37.